

Robotic Guide Dog: Leading a Human with Leash-Guided Hybrid Physical Interaction

Anxing Xiao*, Wenzhe Tong*, Lizhi Yang*, Jun Zeng, Zhongyu Li, and Koushil Sreenath

Abstract—An autonomous robot that is able to physically guide humans through narrow and cluttered spaces could be a big boon to the visually-impaired. Most prior robotic guiding systems are based on wheeled platforms with large bases with actuated rigid guiding canes. The large bases and the actuated arms limit these prior approaches from operating in narrow and cluttered environments. We propose a method that introduces a quadrupedal robot with a leash to enable the robot-guiding-human system to change its intrinsic dimension (by letting the leash go slack) in order to fit into narrow spaces. We propose a hybrid physical Human Robot Interaction model that involves leash tension to describe the dynamical relationship in the robot-guiding-human system. This hybrid model is utilized in a mixed-integer programming problem to develop a reactive planner that is able to utilize slack-taut switching to guide a blind-folded person to safely travel in a confined space. The proposed leash-guided robot framework is deployed on a Mini Cheetah quadrupedal robot and validated in experiments (Video¹).

I. INTRODUCTION

Guide dogs play a critical role in our society by helping the frail, elderly, or visually impaired people navigate the world. However, a well-behaved guide dog usually needs to be selected and trained individually. In addition, the skills from one dog cannot be transferred to another one. This makes training guide dogs both time and labor intensive with the process not easily scalable. With recent progress in robotics, an autonomous robot could potentially take over this responsibility. Our goal in this paper is to create a robotic guide dog. Most previous guide robots have large foot-bases [1]–[3] and usually require an actuated rigid arm to guide the human [4]–[6], which results in limited capabilities of operating in narrow spaces. Moreover, the usage of a rigid arm brings an additional layer of complexity in mechanical and control design. A small robot that could guide humans with a leash could potentially solve such an issue. The ability of the leash to become slack allows the robot to change the internal dimensions of the human-robot system, and thus allows the robot to guide the human through narrow spaces, such as a doorway. However, utilizing a leash could involve a hybrid system switch, i.e., the leash could be taut or slack, which makes this motion planning more challenging. Therefore, we seek to address such a problem where we utilize a quadrupedal robot, a Mini Cheetah [7], to guide a

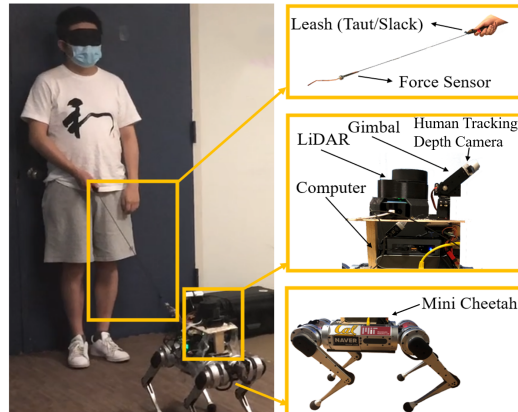


Fig. 1: The Mini Cheetah is guiding a blindfolded person to avoid obstacles with leash-guided assistance: a leash (top right) is used to connect between the robot and the human, a 2D LiDAR is used for robot localization and a depth camera is used for human detection (middle right). The leash could be taut or slack during the navigation.

visually-impaired person via a leash to navigate in narrow spaces, as shown in Fig. 1.

A. Related Work

1) *Robotic Guide Dog*: Using robots to guide humans is a long-studied problem, and the mainstream approaches employ either a robotic cane [4], [5], [8], or a robotic walker [1]–[3]. However, for [4], [5], [8], since they use an actuated rigid arm as a guiding cane between the robot and the human, the system may get stuck in a region which cannot fit the robot arm. Moreover, an actuated arm brings more DoFs and needs additional effort on control and mechanical design. Of the approaches with robot walkers, [1], [2] are designed for the elderly and movement-impaired population and do not consider the visually impaired, and while [3] considers the visually impaired, the guiding system has a very large foot-base. The large base also occurs in [1], [2], and makes maneuvering and guiding a person in a narrow space impossible. Apart from using the movement of a rigid robot arm, different ways to interact between the robot and the human have also been explored, with most methods employing either vocal cues [9], or haptic feedback [10]. Some [5], [6], [11] take it a step further and employ a mix of the methods mentioned above. However, the vocal cues may not always be clear to the people being led, and as previously mentioned, rigid rods decrease the mobility of the system in a confined space significantly. While haptic feedback has been explored in [10], it is only a wearable system with some vibration feedback, and does not consider a system

* Authors have contributed equally.

All authors are with the Department of Mechanical Engineering, University of California, Berkeley, CA, 94720, USA, {xax, wenzhe.t99, lzyang, zengjunsjt, zhongyu.li, koushils}@berkeley.edu

¹Video: <https://youtu.be/FySXRzmji8Y>

containing both a human and a movable robot. Thus, the prior work does not guide a human while also being able to change the intrinsic dimension of the human-robot system.

2) *Hybrid System Planning*: Hybrid system control and planning is challenging for physical human-robot interaction (pHRI) tasks [12]. There is some prior work on hybrid system *control* in pHRI [13], [14]. For path *planning* in pHRI, it was demonstrated in [6], [15]–[17] that a collision-free trajectory could be generated to guide the human. As we introduce a leash for the robot to guide the human, the system becomes hybrid as the leash could be taut or slack. For hybrid modes on leash tension, previous works about aerial systems formulate the path planning either through a special mechanical design [18], mixed-integer programming [19] or collocation-based optimization with complementarity constraints [20], [21]. However, physical human-robot interaction is not considered in [14], [19]–[21], and hybrid path planning for pHRI for applications using mobile robots still remains an open problem.

B. Contributions

We make the following contributions:

- One of the first end-to-end hybrid physical human-robot interaction (hybrid-pHRI) framework is presented for a robotic guide dog with a leash.
- A hybrid model is developed to capture the dynamic relationship in the robot-leash-human system, involving a leash tension model. The hybrid model is validated with experimental data.
- We formulate a mixed-integer programming problem in the path planner to safely guide humans to avoid obstacles during navigation to the goal location while also considering the taut/slack modes of the leash.
- We validate our hybrid-pHRI robot guide framework experimentally on a quadrupedal robot, where a Mini Cheetah is empowered to navigate with a collision-free trajectory in narrow environments while guiding people by exploiting hybrid mode switches.

II. PHYSICAL HUMAN ROBOT INTERACTION (pHRI) MODEL

The ability of the robot to determine the current configuration of the human-robot system and to interact with the human via the leash is very important for successful path planning and guiding a human. Thus a pHRI model is needed to capture the state of the human-robot system and serve as the underlying basis for planning and interaction.

A. Human-robot System

The human-robot system configuration is defined as follows:

$$\mathbf{x}^h = \mathbf{x} - l\mathbf{e}_l, \quad (1)$$

where $\mathbf{x}^h = (x^h, y^h)$ and $\mathbf{x} = (x, y)$ are the position of the human and robot respectively. Furthermore, l represents the distance between the human and the robot and $\mathbf{e}_l = (\cos(\theta - \phi), \sin(\theta - \phi)) \in S^1$ is the unit vector point from the human to the robot along the leash. θ represents the orientation of

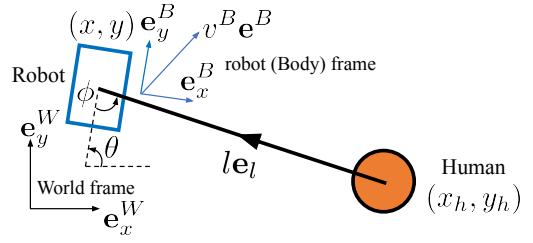


Fig. 2: Configuration of the human-robot guiding system. Human (x^h, y^h) is guided by a leash attached to the robot (x, y) , $l\mathbf{e}_l$ represents the relative position between them.

the robot in the world frame W , and ϕ represents the relative orientation of the human in the robot body frame B . This configuration is valid no matter if the leash is taut or slack, as shown in Fig. 2. When the leash is taut, the system has four degrees-of-freedom with configuration space $Q_t = \mathbb{R}^2 \times S^1$ and $l = l_0$. When the leash is slack, the system has five degrees-of-freedom with configuration space $Q_s = \mathbb{R}^2 \times S^1 \times \mathbb{R}$ and l becomes less than l_0 . Here l_0 is the length of the leash.

B. Hybrid Dynamic Model

1) *Taut Mode*: The assumption for our hybrid dynamic model comes from our intuitive hypothesis that the human will be guided by the robot and move in the direction of the force applied by the leash when the leash is taut. Moreover, when the leash is slack, the human will not feel any force in the leash and thus will not move. Based on this assumption, we define our hybrid system with continuous-time generalized coordinates $\mathbf{q} = (x, y, \theta, \phi, l) \in \mathbb{R}^5$ and with an input of $\mathbf{u} = (\mathbf{v}^B, \omega) \in \mathbb{R}^3$, where $\mathbf{v}^B = v^B \mathbf{e}^B$ represents the robot velocity in its body frame, shown in Fig. 2. The robot velocity \mathbf{v}^B and angular velocity ω are the commands which could be sent to the Mini Cheetah directly and a tracking controller could track these commands.

When the leash becomes taut, based on our assumption and the geometric relationship, the hybrid dynamics $\dot{\mathbf{q}}_t = f_t(\mathbf{q}_t, \mathbf{u}_t)$ could be formulated as follows,

$$\dot{x} = \alpha_x v^B \mathbf{e}^B \cdot \mathbf{e}_x^W, \quad (2a)$$

$$\dot{y} = \alpha_y v^B \mathbf{e}^B \cdot \mathbf{e}_y^W, \quad (2b)$$

$$\dot{\theta} = \alpha_\theta \omega, \quad (2c)$$

$$\dot{\phi} = -\alpha_\theta \omega - \alpha_\phi \|v^B \mathbf{e}^B \times \mathbf{e}_l\| / l_0, \quad (2d)$$

$$l = l_0, \quad (2e)$$

shown in the left mode in Fig. 3.

The human-robot interaction and inelastic collision when the leash switches from slack to taut is very hard to model and this external force brings disturbance for the robot tracking controller. To compensate these tracking errors from this disturbance, we introduce

$$\alpha = [\alpha_x, \alpha_y, \alpha_\theta, \alpha_\phi] \in [0, 1]^4 \quad (3)$$

as the discount coefficients in (4). These discount coefficients are smaller than one since human always tend to drag the leash from the opposite direction with respect to the

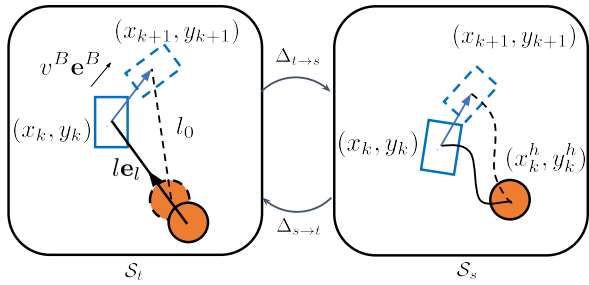


Fig. 3: Hybrid modes switches in the discrete dynamics model Σ . The hybrid modes switches from \mathcal{S}_s to \mathcal{S}_t when leash becomes taut and the switch action is denoted as $\Delta_{s \rightarrow t}$. When the cable becomes slack, it switches back to \mathcal{S}_s with action denoted as $\Delta_{t \rightarrow s}$. This hybrid mode transitions are shown in the discrete-time manner.

commands to the robot, i.e., $v^B \mathbf{e}^B$ and ω . These discount coefficients allow us to capture the unknown interaction acting on the robot from the human with a four-dimension representation and these four coefficients which can be tuned for a good prediction.

2) *Slack Mode*: When the leash is slack, the hybrid dynamics $\dot{\mathbf{q}}_s = f_s(\mathbf{q}_s, \mathbf{u}_s)$ can be defined as follows,

$$\dot{x} = v^B \mathbf{e}^B \cdot \mathbf{e}_x^W, \quad (4a)$$

$$\dot{y} = v^B \mathbf{e}^B \cdot \mathbf{e}_y^W, \quad (4b)$$

$$\dot{\theta} = \omega, \quad (4c)$$

$$\dot{\phi} = -\|v^B \mathbf{e}_l \times \mathbf{e}^B\|/l_0, \quad (4d)$$

$$\dot{l} = v^B \mathbf{e}_l \cdot \mathbf{e}^B, \quad (4e)$$

where (4d), (4e) comes from the geometric relation. where only the robot is moving since the cable is slack, shown in the right mode in Fig. 3.

C. Leash Tension Model

We seek a simple mapping from generalized coordinates to the leash tension, which allows for the consideration of physical interaction during the path planning. To capture the relation between generalized coordinates and leash tension, we construct a linear regression model between robot speed and leash tension to minimize mean squared errors.

$$F = F_{\text{MSE}}(\mathbf{q}_t) = \beta_1 \mathbf{v}^B \cdot \mathbf{e}_l + \beta_2, \quad (5)$$

where $\mathbf{v}^B \cdot \mathbf{e}_l$ represents the projected speed of robot along the taut leash direction and could be expressed by the generalized coordinates \mathbf{q}_t with simple calculations, as proven by experiments in V.

D. Hybrid Modes Transition

Since a taut leash is almost analogous to a rigid arm and thus infeasible in confined spaces due to the increased size of the human-robot system, the leash will need to transition to slack mode, and a hybrid system is introduced into the model. We consider the following hybrid system Σ as follows,

$$\Sigma = \begin{cases} \dot{\mathbf{q}}_t = f_t(\mathbf{q}_t, \mathbf{u}_t), & \mathbf{q}_t \notin \mathcal{S}_s \\ \mathbf{q}_s^+ = \Delta_{s \rightarrow t}(\mathbf{q}_t^-), & \mathbf{q}_t^- \in \mathcal{S}_s \\ \dot{\mathbf{q}}_s = f_s(\mathbf{q}_s, \mathbf{u}_s), & \mathbf{q}_s \notin \mathcal{S}_t \\ \mathbf{q}_t^+ = \Delta_{t \rightarrow s}(\mathbf{q}_s^-), & \mathbf{q}_s^- \in \mathcal{S}_t \end{cases} \quad (6)$$

The dynamics for two hybrid modes are shown in (2) and (4). The two hybrid regions \mathcal{S}_t and \mathcal{S}_s are defined as follows,

$$\mathcal{S}_t = \{(\mathbf{q}_t, F) \in \mathbb{R}^6 : \mathbf{e}_l \cdot \mathbf{e}^B \geq 0 \wedge F \geq \bar{F}\} \quad (7)$$

$$\mathcal{S}_s = \{(\mathbf{q}_s, F) \in \mathbb{R}^6 : \mathbf{e}_l \cdot \mathbf{e}^B \leq 0 \vee F \leq \bar{F}\} \quad (8)$$

where $\mathbf{e}_l \cdot \mathbf{e}^B < 0$, the robot and the human will approach each other in next time step which will make the leash slack. Moreover, \bar{F} is applied as the lower bound representing the maximum intrinsic leash tension when the leash is slack.

III. PATH PLANNING WITH HYBRID PHYSICAL HUMAN ROBOT INTERACTION

In this section, we discuss our optimization-based path planning algorithm where we consider the hybrid physical human robot interaction. We are given current coordinates \mathbf{q}_{curr} and target goal coordinates \mathbf{q}_{target} generated in the path from a global planner, which will be described in Sec. IV-B. A mixed-integer collocation-based problem along a horizon N with time step $\Delta t = t/N$ is formulated as follows,

$$\min L(\mathbf{q}_k, \mathbf{u}_k, s_k, t) \quad \text{subject to} \quad (9a)$$

$$\mathbf{q}_0 = \mathbf{q}_{curr}, \quad (9b)$$

$$\mathbf{q}_{k+1} = \bar{f}_t(\mathbf{q}_k, \mathbf{u}_k), \quad \text{if } s_k = 1 \quad (9c)$$

$$\mathbf{q}_{k+1} = \bar{f}_s(\mathbf{q}_k, \mathbf{u}_k), \quad \text{if } s_k = 0 \quad (9d)$$

$$s_k = 1, \quad \text{if } \mathbf{e}_l(\mathbf{q}_k) \cdot \mathbf{e}^B(\mathbf{q}_k) \geq 0 \wedge F_k \geq \bar{F} \quad (9e)$$

$$s_k = 0, \quad \text{otherwise} \quad (9f)$$

$$F_l(\mathbf{q}_k) \leq F_k \leq F_u(\mathbf{q}_k), \quad (9g)$$

$$\mathbf{q}_l \leq \mathbf{q}_k \leq \mathbf{q}_u, \quad (9h)$$

$$\mathbf{u}_l \leq \mathbf{u}_k \leq \mathbf{u}_u, \quad (9i)$$

where \bar{f}_t and \bar{f}_s represent the discrete dynamics with sampling time step $\Delta t = t/N$. Furthermore, $s_k \in \{0, 1\}$ is the variable describing the hybrid dynamical mode in (9c) and (9d) and s_k equals to one when the cable is taut and zero when the cable is slack, shown in (9e) and (9f). The state, input and force constraints are imposed in (9h) and (9i) and (9g). Notice that \mathbf{e}_l and \mathbf{e}^B could be expressed as functions of the generalized coordinates \mathbf{q}_k at each time step, which was discussed in Sec. II-B. This nonlinear collocation-based optimization problem is formulated in CasADi [22] with logic to switch modes and is solved with IPOPT [23].

A. Cost Function

We define the cost function (9a) as follows,

$$L(\mathbf{q}_k, \mathbf{u}_k, s_k, t) = \|\mathbf{q}_N - \mathbf{q}_{target}\|_{\mathbf{Q}_{target}} + S_t t + \sum_{k=0}^{N-1} (\|\mathbf{u}_k\|_{\mathbf{Q}_u} + S_F F_k + S_l(l_0 - l_k) + S_{\Delta F}(F_{k+1} - F_k)) \quad (10)$$

where we have $\mathbf{Q}_{target} \in \mathbb{R}^5$, $\mathbf{Q}_u \in \mathbb{R}^3$ as positive definite and $S_F, S_{\Delta F}, S_l$ as positive scalars. We have two terminal cost terms and four stage cost terms. The term $\|\mathbf{q}_N - \mathbf{q}_{target}\|_{\mathbf{Q}_{target}}$ represents the quadratic terminal cost which tries to minimize the deviation of the final node from the target position. We do not assert a hard constraint for

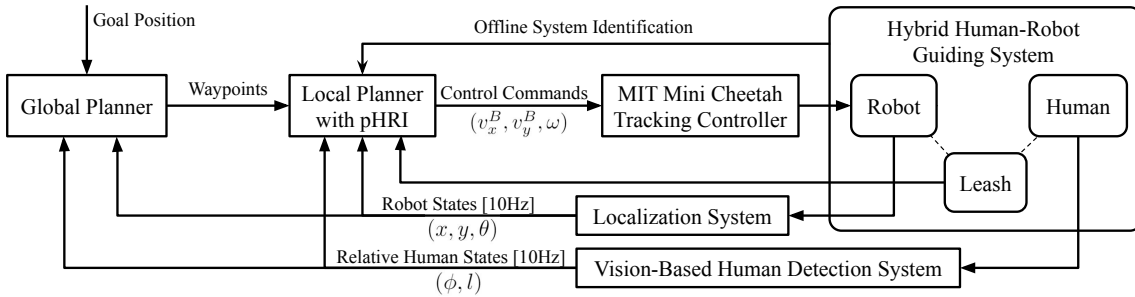


Fig. 4: Framework for the Mini Cheetah robotic guide dog. Given the current position and goal position, a global planner using A* algorithm generates target feasible waypoints for the local planner. Then the local planner generates a short trajectory and sends control commands to the robot.

reaching the target position and it allows us more feasibility in the optimization. The term $S_t t$ allows us to find an optimal travel time for robot motions instead of using a fixed value.

For the stage cost, $\|\mathbf{u}_k\|_{\mathbf{Q}_u}$ minimizes the control input, $S_F F_k$ minimizes the leash tension while ensuring smooth tension change with additional cost $S_{\Delta F}(F_{k+1} - F_k)$. The term $S_l(l_0 - l_k)$ brings us faster optimization convergence and it tends to have more taut modes, which helps to guide the guided person since the person is immobile when $l_k < l_0$.

B. Data-driven Leash Tension Constraint

In our leash tension model (5) in Sec. II-C, we have seen that we have a mapping from the generalized coordinates to the leash tension. During the implementation of our collocation-based problem (9), instead of adding this mapping relation as a constraint, we impose lower and upper bounds on this mapping, where we have

$$F_l(\mathbf{q}_k), F_u(\mathbf{q}_k) = F_{\text{MSE}}(\mathbf{q}_k) \pm \sigma(F_{\text{MSE}}), \quad (11)$$

where $\sigma(F_m)$ represents the standard deviation of the linear regression in our leash tension model (5). Notice that imposing a two-sided constraint brings larger feasibility compared to an equality constraint. This force constraint allows us to consider the physical human-robot interaction in the planner.

C. Obstacle Avoidance

When the system is required to navigate in an environment with obstacles, our optimization problem in (9) is no longer sufficient and obstacle avoidance constraints need to be added. In this paper, we consider the obstacle avoidance for both the robot and the human, where two simple signed distance constraints are imposed on them. Assume the j -th obstacle is located at $\mathbf{x}_k^{\text{obs},j} = (x_k^{\text{obs},j}, y_k^{\text{obs},j})$ at time step k . We then have,

$$\|\mathbf{x}_k - \mathbf{x}_k^{\text{obs},j}\| \geq d + r + r_j^{\text{obs}}, \quad (12)$$

$$\|\mathbf{x}_k^h - \mathbf{x}_k^{\text{obs},j}\| \geq d + r^h + r_j^{\text{obs}}, \quad (13)$$

where r , r^h and r_j^{obs} represent the robot, human and obstacle dimensions. We also add a safety margin d which allows us to ensure safety while handling our state-estimation and tracking errors.

IV. QUADRUPEDAL ROBOTIC GUIDE SYSTEM

A. Framework

To safely navigate and guide a visually-blind person in a cluttered environment, an end-to-end framework is constructed and illustrated in Fig. 4. Our planner is composed of a search-based A* global planner and a collocation-based local planner with physical human robot interaction, as introduced in the previous section.

B. Global Planner

For the global planner, we use a search-based A* planner over the grid map on a reduced generalized coordinates $\tilde{\mathbf{x}} = (x, y, \phi) \in \mathbb{R}^3$. The continuous transition between nodes on the \mathbb{R}^3 configuration space is defined as $(\Delta x, \Delta y, \Delta \phi)$. For experiments, we have $\Delta x = \pm 0.5$, $\Delta y = \pm 0.25$ and $\Delta \phi = \pm \pi/8$. The node cost and heuristic cost to-go at node $\tilde{\mathbf{x}}_n$ are defined as $g(\tilde{\mathbf{x}}_n)$ and $h(\tilde{\mathbf{x}}_n)$ where,

$$g(\tilde{\mathbf{x}}_n) = \sum_{i=1}^{N-1} \|\tilde{\mathbf{x}}_n - \tilde{\mathbf{x}}_{n-1}\|^2 \quad (14)$$

$$h(\tilde{\mathbf{x}}_n) = \|x_N - x_{\text{goal}}\|^2 + \|y_N - y_{\text{goal}}\|^2 + \|\phi_N - \phi_{\text{goal}}\|^2 + \lambda(1 - \cos(\theta_N - \theta_{\text{goal}})), \quad (15)$$

where θ_N can be calculated with approximate dynamics (9c) using continuous transition between nodes while assuming the leash is always taut. A cosine function is applied on θ in the heuristic cost to-go to solve the singularity problem. This A* global planner generates a continuous collision-free trajectory with a sequence of 5-dimensional waypoints. This is passed to the local planner with pHRI introduced in Sec. III.

C. Robot Localization And Human Tracking

Knowing robot and human states online is critical for the autonomous system. We firstly build an occupancy grid map with a 2D lidar based on Hector Slam [24]. Later, AMCL [25] is utilized to estimate the robot states in the world frame. To estimate the position of the guided person, a Depth-RGB camera is used to detect the human's 3D position through OpenVINO [26] and a Kalman Filter based on a constant-speed linearized system [6] is applied to track the detected human position. The camera is deployed on a 2 DoF gimbal which can rotate and pitch. This camera gimbal is mounted

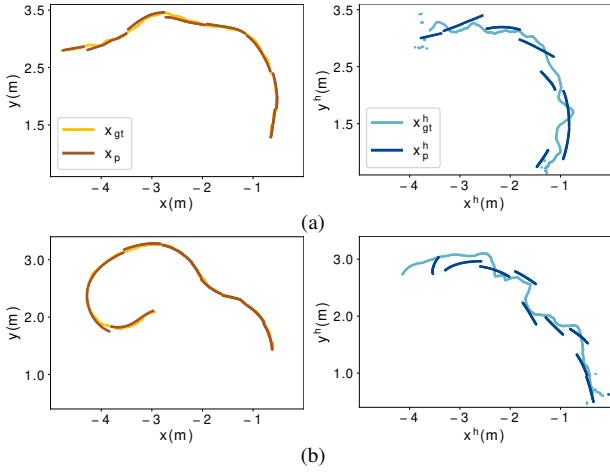


Fig. 5: Two typical guiding test cases for optimizing the human-robot dynamic model by minimizing the error of ground truth robot position \mathbf{x}_{gt} and model-based computed robot position \mathbf{x}_p . Fig. 5a and Fig. 5b are two separate test cases, with the robot trajectory on the left and the human trajectory on the right.

on the robot’s top surface and is programmed to keep the guided person visible in the camera frame irrespective of the relative orientation of the human with respect to the robot.

D. Velocity Tracking Controller on Mini Cheetah

We use the existing state of the art velocity tracking controller for Mini Cheetah, where a MPC [27] computes desired ground reaction forces and desired foot and body position from given velocity commands. From these desired contact forces, WBIC [28] computes desired joint position velocity that are delivered to joint-level controllers to generate joint torques.

V. EXPERIMENTS AND EVALUATION

The hardware setup is illustrated in Fig. 1. and all the aforementioned proposed algorithms are running on an on-board Intel computer using ROS, while the velocity tracking controller is running on a real-time computer within the Mini Cheetah.

A. Offline System Identification

1) *Human-robot dynamic model*: The discount coefficients α in (3) in Sec. II-B for the taut mode of human-robot dynamic are first identified based on offline experimental data. In order to obtain such data, several blind-folded people are guided in an unknown environment along various trails. In each trail, a human operator commands the Mini Cheetah to randomly move around while ensuring a taut leash. In such experiments, robot global positions \mathbf{x}_{gt} and human positions \mathbf{x}_{gt}^h are recorded along the sample trajectories, serving as ground truth data, and α is sampled in the range of $[0, 1]$. With each set of these sampled values, we compute the predicted robot global positions, denoted as \mathbf{x}_p , based on the dynamic model of the taut mode (2). The value of α that can produce the smallest least mean squared distance between the predicted and estimated trajectories are picked. The identified value of α is $[0.8, 0.8, 0.6, 0.8]$, which was

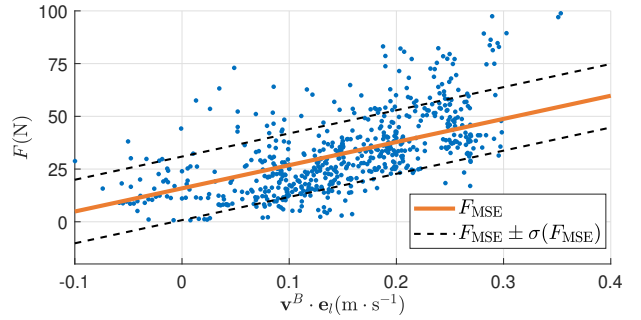


Fig. 6: Validating leash tension model in Eq. (5) by randomly walking. Linear regression is carried out between the projected speed in the leash direction $\mathbf{v}^B \cdot \mathbf{e}_l$ and leash tension F . As shown, 76% of the measured tension data lies between $F_m \pm \sigma(F_m)$. Furthermore, $\sigma(F_m)$ represents the standard deviation of this linear regression.

obtained by minimizing the prediction error for the human-robot system. This is incorporated in the dynamic model for later human guiding experiments.

The ground truth and predicted trajectories are illustrated by the identified α in Fig. 5. The identification of the dynamic model of taut mode matches well between the ground truth robot position \mathbf{x}_{gt} and the predicted robot position \mathbf{x}_p , with an average prediction error of 0.023m. The human prediction error is 0.176m, which is acceptable, considering the noise of human detection and estimation.

2) *Leash Tension Model*: The leash tension model given by (5) in Sec. II-C is validated by letting the robot guide a human via a leash to move randomly, with the leash being either slack and taut. The interactive force F , system states and control commands (\mathbf{v}^B, ϕ) are recorded. The projected velocity along the leash direction $\mathbf{v}^B \cdot \mathbf{e}_l(\phi)$ is later obtained.

We fit our force F with a linear model (5) while minimizing the least square errors, shown in Fig. 6. The reasons for choosing a linear model over higher-order ones are two-fold: during experiments higher-order models did not exhibit superior prediction performance and a linear model reduces complexity in the optimization-based local planner. The parameters we optimized are $\beta_1 = 109.8$ and $\beta_2 = 15.85$. The standard deviation of force is $\sigma(F_{MSE}) = 15.06$, which was used for estimating lower and upper bounds of force constraints (9g). We verify that 76% of our force data lies between the region constrained with our linear regression model and related standard deviation, which is acceptable for estimating the force constraints.

B. Robot Guiding Human Experiments

The proposed system is evaluated in various maps of narrow spaces. One such example is shown in Fig. 7, where the map consists of a narrow doorway connected to a narrow corridor, with the narrowest traversal region being only of width 1.0 m. Since the human-robot system has a length of 1.6 m when the leash is taut and the human only moves along the direction of the force, it is hard for the human-robot system to pass through this region if the leash stays taut. This allows for the demonstration of the hybrid mode switch in our local planner. This map contains several situations the

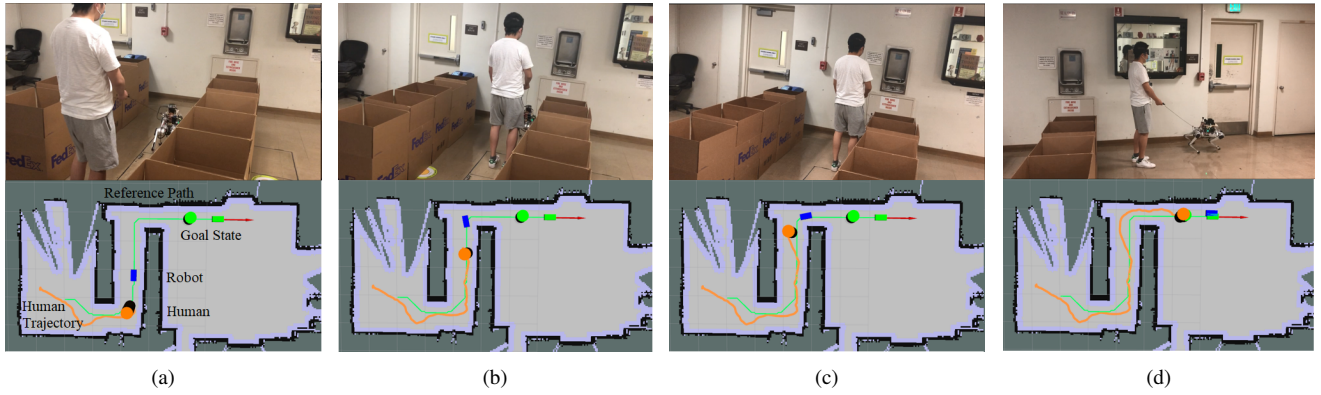


Fig. 7: Snapshot of the guiding process. The Mini Cheetah guides a blindfolded person from an initial to a target position. The blue marker and orange marker represent the robot and human. Human history trajectory is represented by the orange line while the robot global planned reference is represented by the green line.

system will face in the real world including doors, narrow corridors and corners.

The experimental goal is to enable the Mini-cheetah to safely guide a blindfolded person to the given goal location \mathbf{q}_{goal} without colliding with obstacles. To evaluate the performance of our planning system, we choose the several different goal locations far from the different initial locations and let the robot plan and control fully autonomously. Three adults participated in the experiments in this narrow map. In the experiments, the human-robot system successfully reached the given goal without any collision.

For the example experiment shown in Fig. 7, the time the Mini Cheetah took to guide the blindfolded person to the random final goal position is roughly 75s. In this map, the leash switched to taut at the beginning part of the task. When the human-robot system came to the most narrow region of the second doorway, the leash switched to slack mode and the guided human stopped moving as shown in Fig. 7c. After the robot changed its configuration that allowed it to guide the human pass the narrow region, the human-robot system switched to the taut mode and passed this doorway as shown in Fig. 7d.

Moreover, as shown in Fig. 8a, the tension threshold \bar{F} measured at the beginning of experiment is 12 N. We notice that from 45s to 60s, when the human-robot system approached the narrow space of the second doorway, the force in the leash was extremely small as the system switched into slack mode, and the robot was changing its individual configuration until it was able to guide the human pass the doorway. In this period, the human was not pulled by the robot and stopped moving, as shown by the fact that the speed of human movement was near zero (0.05m/s) between 45s to 60s. After 60s, the robot changed its position and orientation to a suitable state, switching to taut mode to apply the leash force again to guide the human to the final goal position.

VI. CONCLUSION AND FUTURE WORK

To our knowledge, this work proposes one of the first end-to-end human-robot interaction system to serve as an autonomous navigation aid to enable the visually impaired

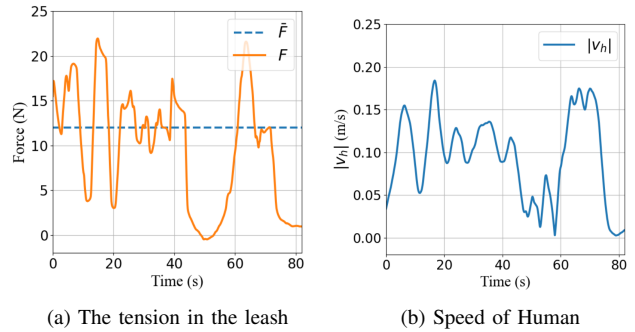


Fig. 8: Experimental results of the tension in the leash and human speed. \bar{F} represents the threshold of the force. From 45s-60s, the force in the leash in (a) is nearly 0 N (implicating a slack leash) and the human moving speed is also below 0.05 m/s in (b).

to traverse narrow and cluttered spaces. A data-driven interaction force model and a hybrid dynamic model were developed to help plan paths with hybrid mode switches to switch between taut and slack states for the leash. A global planner along with a mixed-integer optimization-based local planner were formulated to generate trajectories that served as input to the low-level controller on the Mini Cheetah. The proposed pipeline was deployed on the Mini Cheetah and validated by experiments with a blind-folded person. Experimental results indicate that our system is able to physically guide the person with a safe and efficient trajectory in a narrow space, including obstacle avoidance maneuvers and hybrid state transitions. Future work will focus on more complicated modeling of human behavior with force traction to propose more novel applications of the robotic guide dog.

ACKNOWLEDGEMENT

This work is supported in part by the National Science Foundation Grants CMMI-1944722. The authors would also like to thank Professor Sangbae Kim, the MIT Biomimetic Robotics Lab, and NAVER LABS for providing the Mini Cheetah simulation software and lending the Mini Cheetah for experiments.

REFERENCES

- [1] A. Morris, R. Donamukkala, A. Kapuria, A. Steinfeld, J. T. Matthews, J. Dunbar-Jacob, and S. Thrun, "A robotic walker that provides guidance," in *IEEE International Conference on Robotics and Automation (Cat. No. 03CH37422)*, vol. 1, 2003, pp. 25–30.
- [2] L. Palopoli, A. Argyros, J. Birchbauer, A. Colombo, D. Fontanelli, A. Legay, A. Garulli, A. Giannitrapani, D. Macii, F. Moro, P. Nazemzadeh, P. Padeleris, R. Passerone, G. Poier, D. Prattichizzo, T. Rizano, L. Rizzon, S. Scheggi, and S. Sedwards, "Navigation assistance and guidance of older adults across complex public spaces: the dali approach," *Intelligent Service Robotics*, vol. 8, pp. 77–92, 04 2015.
- [3] A. Wachaja, P. Agarwal, M. Zink, M. R. Adame, K. Möller, and W. Burgard, "Navigating blind people with walking impairments using a smart walker," *Autonomous Robots*, vol. 41, no. 3, pp. 555–573, 2017.
- [4] J. Borenstein and I. Ulrich, "The guidecane—a computerized travel aid for the active guidance of blind pedestrians," in *Proceedings of International Conference on Robotics and Automation*, vol. 2, 1997, pp. 1283–1288.
- [5] T.-K. Chuang, N.-C. Lin, J.-S. Chen, C.-H. Hung, Y.-W. Huang, C. Teng, H. Huang, L.-F. Yu, L. Giarré, and H.-C. Wang, "Deep trail-following robotic guide dog in pedestrian environments for people who are blind and visually impaired—learning from virtual and real worlds," in *IEEE International Conference on Robotics and Automation*, 2018, pp. 1–7.
- [6] Z. Li and R. Hollis, "Toward a ballbot for physically leading people: A human-centered approach," in *IEEE/RSJ International Conference on Intelligent Robots and Systems*, 2019, pp. 4827–4833.
- [7] B. Katz, J. Di Carlo, and S. Kim, "Mini cheetah: A platform for pushing the limits of dynamic quadruped control," in *International Conference on Robotics and Automation*, 2019, pp. 6295–6301.
- [8] C. Ye, S. Hong, X. Qian, and W. Wu, "Co-robotic cane: A new robotic navigation aid for the visually impaired," *IEEE Systems, Man, and Cybernetics Magazine*, vol. 2, no. 2, pp. 33–42, 2016.
- [9] L. Yang, I. Herzi, A. Zakhori, A. Hiremath, S. Bazargan, and R. Tames-Gadam, "Indoor query system for the visually impaired," in *ICCHP*, 2020.
- [10] R. Katzschmann, B. Araki, and D. Rus, "Safe local navigation for visually impaired users with a time-of-flight and haptic feedback device," *IEEE Transactions on Neural Systems and Rehabilitation Engineering*, vol. PP, pp. 1–1, 01 2018.
- [11] D. Dakopoulos and N. G. Bourbakis, "Wearable obstacle avoidance electronic travel aids for blind: A survey," *IEEE Transactions on Systems, Man, and Cybernetics, Part C (Applications and Reviews)*, vol. 40, no. 1, pp. 25–35, 2010.
- [12] A. Pervez and J. Ryu, "Safe physical human robot interaction—past, present and future," *Journal of Mechanical Science and Technology*, vol. 22, no. 3, p. 469, 2008.
- [13] A. J. Del-Ama, J. C. Moreno, A. Gil-Agudo, A. De-los Reyes, and J. L. Pons, "Online assessment of human-robot interaction for hybrid control of walking," *Sensors*, vol. 12, no. 1, pp. 215–225, 2012.
- [14] E. Magrini and A. De Luca, "Hybrid force/velocity control for physical human-robot collaboration tasks," in *IEEE/RSJ International Conference on Intelligent Robots and Systems*, 2016, pp. 857–863.
- [15] I. Ulrich and J. Borenstein, "Vfh/sup*: Local obstacle avoidance with look-ahead verification," in *IEEE International Conference on Robotics and Automation*, 2000, pp. 2505–2511.
- [16] V. Kulyukin, C. Gharpure, J. Nicholson, and G. Osborne, "Robot-assisted wayfinding for the visually impaired in structured indoor environments," *Autonomous Robots*, vol. 21, no. 1, pp. 29–41, 2006.
- [17] L. Palopoli, A. Argyros, J. Birchbauer, A. Colombo, D. Fontanelli, A. Legay, A. Garulli, A. Giannitrapani, D. Macii, F. Moro *et al.*, "Navigation assistance and guidance of older adults across complex public spaces: the dali approach," *Intelligent Service Robotics*, vol. 8, no. 2, pp. 77–92, 2015.
- [18] J. Zeng, P. Kotaru, and K. Sreenath, "Geometric control and differential flatness of a quadrotor uav with load suspended from a pulley," in *2019 American Control Conference (ACC)*. IEEE, 2019, pp. 2420–2427.
- [19] S. Tang and V. Kumar, "Mixed integer quadratic program trajectory generation for a quadrotor with a cable-suspended payload," in *IEEE International Conference on Robotics and Automation*, 2015, pp. 2216–2222.
- [20] P. Foehn, D. Falanga, N. Kuppuswamy, R. Tedrake, and D. Scaramuzza, "Fast trajectory optimization for agile quadrotor maneuvers with a cable-suspended payload," in *Robotics: Science and Systems*, 2017.
- [21] J. Zeng, P. Kotaru, M. W. Mueller, and K. Sreenath, "Differential flatness based path planning with direct collocation on hybrid modes for a quadrotor with a cable-suspended payload," *IEEE Robotics and Automation Letters*, vol. 5, no. 2, pp. 3074–3081, 2020.
- [22] J. A. Andersson, J. Gillis, G. Horn, J. B. Rawlings, and M. Diehl, "Casadi: a software framework for nonlinear optimization and optimal control," *Mathematical Programming Computation*, vol. 11, no. 1, pp. 1–36, 2019.
- [23] L. T. Biegler and V. M. Zavala, "Large-scale nonlinear programming using ipopt: An integrating framework for enterprise-wide dynamic optimization," *Computers & Chemical Engineering*, vol. 33, no. 3, pp. 575–582, 2009.
- [24] S. Kohlbrecher, J. Meyer, O. von Stryk, and U. Klingauf, "A flexible and scalable slam system with full 3d motion estimation," in *IEEE International Symposium on Safety, Security and Rescue Robotics*, November 2011.
- [25] D. Fox, W. Burgard, F. Dellaert, and S. Thrun, "Monte carlo localization: Efficient position estimation for mobile robots," in *Proceedings of the Sixteenth National Conference on Artificial Intelligence.*, July 1999.
- [26] Y. Gorbachev, M. Fedorov, I. Slavutin, A. Tugarev, M. Fatekhov, and Y. Tarkan, "Openvino deep learning workbench: Comprehensive analysis and tuning of neural networks inference," in *Proceedings of the IEEE/CVF International Conference on Computer Vision (ICCV) Workshops*, Oct 2019.
- [27] J. Di Carlo, P. M. Wensing, B. Katz, G. Bledt, and S. Kim, "Dynamic locomotion in the mit cheetah 3 through convex model-predictive control," in *IEEE/RSJ International Conference on Intelligent Robots and Systems*, 2018, pp. 1–9.
- [28] D. Kim, J. Di Carlo, B. Katz, G. Bledt, and S. Kim, "Highly dynamic quadruped locomotion via whole-body impulse control and model predictive control," *arXiv preprint arXiv:1909.06586*, 2019.